Chinese Chemical Letters 31 (2020) 841–845

Contents lists available at ScienceDirect

Chinese Chemical Letters

journal homepage: www.elsevier.com/locate/cclet

Communication

In situ [2 + 3] cycloaddition synthesis, crystal structures, strong SHG responses and fluorescence properties of three novel Zn coordination polymers

Haitao Zhou, Kang Yang, Yao Liu, Yunzhi Tang, Wenjuan Wei, Qing Shu, Jinjun Zhao, Yuhui Tan*

School of Metallurgy and Chemical Engineering, Jiangxi University of Science and Technology, Ganzhou 341000, China

ARTICLE INFO

Article history:
Received 3 April 2019
Received in revised form 3 June 2019
Accepted 10 June 2019
Available online 11 June 2019

Keywords:
In situ synthesis
Tetrazole complexes
Zinc complex
SHG responses
Luminescence properties

ABSTRACT

We report on the synthesis of two acentric and one centrosymmetric Zn metal–organic complexes with 3-tetrazolemethyl pyridine spacers obtained *in situ* by hydrothermal routes. X-ray diffraction structural analysis reveals that they have the same equivalent nodes but with dissimilar topologies. The two acentric frameworks $[Zn(Tzmp)Cl]_n$ (**1**) and $([Zn(Tzmp)Br]_n$ (**2**), HTzmp = 3-tetrazolemethyl pyridine) are isomorphism which exhibit an acentric 3D framework with (10, 3)-b net called "ths", while the centrosymmetric complex ($[Zn(Tzmp)N_3]_n$ (**3**)) features a distinctive 2D sheet with Shubnikov hexagonal plane net. Photo-luminescent studies suggest the ligand-field strength of coordinated negative ions ($Cl^- > Br^- > N_3^-$) has ordered adjusting effects on the emission redshift. The second harmonic generation (SHG) measurement shows that compounds **1** and **2** are nonlinear optically active, with SHG responses being 2/3 and half of the standard potassium dihydrogen phosphate (KDP), respectively.

The essence of systematic MOFs chemistry (reticular chemistry) is the combination of a given metal-containing SBU with a variety of organic SBUs. As Cory *et al.* point out, even both the metal and organic ligands have the same coordination modes and with the similar equivalent nodes such as (3, 3)-connected network, they maybe form different underlying topologies and have total different topologies. Because of the flexibility of design of these organic components (ligands), it is more important to identify all the branching points (vertices) and individual links (edges) rather than just identifying the points of extension [1–4]. Up to date, there have been a few living examples reported with different topologies that made up of the same metal, organic ligands and equivalent nodes before such as ZIF-6 with GIS topology and ZIF-10 with MER topology [4]. However, there were few analogous tetrozle complexes reported because it is very difficult to speculate the effects of synthesis conditions (*e.g.*, auxiliary ligands, temperature, pH) on the final structure [5–9].

Tetrazoles have attracted increasing attention in coordination chemistry due to the excellent coordination ability of the four nitrogen atoms of the functional group to act as either a multidentate or a bridging building block [10–15]. What is more, a lot of investigations have been suggested that different conditions such as negative ions, temperature and pH value have a significant influence on their topological structures of MOFs [14,16–19]. As a systematical work to research the impact of different auxiliary ligands (including halogen, azide, *etc.*) on their topological structures of metal-tetrazole coordination polymers, and explore their application in material field such as luminescence and nonlinear optical, we devour to design some new tetrazole MOFs by selecting different negative ions of the same metal salts as reaction substrate [20–23].

Fortunately, when we use $Zn(ClO_4)_2$ to replac $ZnCl_2$ (or $ZnBr_2$) in the Sharpless reaction of 3-cyanomethyl pyridine with sodium azide, we successfully got three novel Zn-tetrazole complexes, $[Zn(Tzmp)Cl]_n$ (**1**), $[Zn(Tzmp)Br]_n$ (**2**) and $[Zn(Tzmp)N_3]_n$ (**3**). Particularly worth mentioning is that two acentric structures (**1** and **2**) exhibit strong SHG response of 4 and 3 times that of KH_2PO_4 (KDP) respectively and a wide transparency range with a short UV cutoff edge below 300 nm [24–32]. Furthermore, all the title MOFs display strong fluorescent properties which are influenced by the ligand-field strength of the negative ions.

All the reagents and solvents for synthesis were purchased from commercial sources and used as supplied without further purification. As shown in Scheme 1, MOFs **1**, **2** and **3** were

* Corresponding author.
E-mail address: tyxcn@163.com (Y. Tan).

https://doi.org/10.1016/j.cclet.2019.06.017

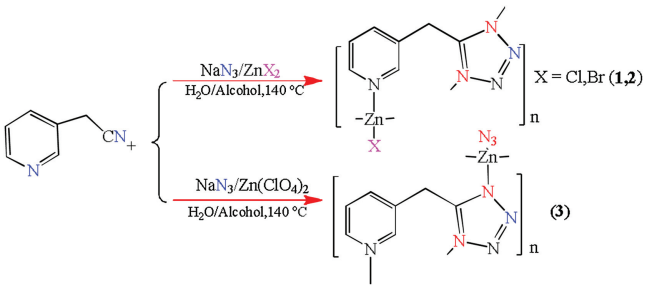

Scheme 1. The preparation of MOFs **1**, **2** and **3**.

prepared under hydrothermal reaction condition. A heavy walled Pyrex tube containing a mixture of 3-cyanomethyl pyridine (0.0236 g, 0.2 mmol), $ZnCl_2$ (0.0272 g, 0.2 mmol) or $ZnBr_2$ (0.0446 g, 0.2 mmol) or $Zn(ClO_4)_2{\cdot}6H_2O$ (0.074 g, 0.2 mmol), and NaN_3 (0.013 g, 0.2 mmol) for **1**, NaN_3 (0.013 g, 0.2 mmol) for **2**, NaN_3 (0.026 g, 0.4 mmol) for **3** and a mixture of water (2 mL) and alcohol (0.5 mL) was frozen and sealed under vacuum, and then placed inside an oven at 140 °C. The colorless crystals for **1**, **2** and **3** were obtained after 24 h of heating. The [2 + 3] cycloadditions are evidenced by the absence of the cyano group peak in the 2244 cm^{-1} region and the presence of the several typical tetrazolyl group peaks ranging from 1613 cm^{-1} to 1451 cm^{-1} in the IR spectra of **1** to **3** (Fig. S1 in Supporting information) [6,33]. The powder X-ray diffraction of their products shows that it is very highly crystalline, since their simulated PXRD pattern based on the crystal structure analysis allowed unambiguous identification *via* a comparison of the experimental and computed powder diffraction patterns (Fig. S2 in Supporting information). For **1**, Yield, 0.0412 g, 78.9%, $C_7H_6ClN_5Zn$ (260.99); For **2**, Yield, 0.0503 g, 82.3%, $C_7H_6BrN_5Zn$ (305.45); For **3**, Yield, 0.0241 g, 45.1%, $C_7H_6ZnN_8$ (267.57) on the basis of organic ligand. Calcd. for **1**, C, 32.19; H, 2.30; N, 26.82; Found for **1**: C, 32.21; H, 2.31; N, 26.76; Calcd. for **2**, C, 27.50; H,1.96; N, 22.92; Found for **2**: C, 27.48; H, 1.97; N, 22.96; Calcd. for **3**, C, 31.39; H, 2.24; N, 41.86; Found for **3**: C, 31.38; H, 2.21; N, 41.90.

Elemental analyses were determined on a Vario EL III elemental analyzer. The Fourier transform infrared (FT-IR) spectra were measured as KBr pellets on a Nicolet Magna 750 FT-IR spectrometer in the range of 4000 – 400 cm^{-1}. Powder X-ray diffraction (PXRD) patterns were collected in the 2θ range of 5°–40° with a scan step of 0.05° in a sealed glass capillary on a Rigaku MiniFlex diffractometer. The fluorescence measurements were performed on an Edinbergh Analytical FLS920 instrument. The UV absorption and optical diffuse-reflectance spectra were measured at room temperature with a PE Lambda 900 UV-vis spectrophotometer. The absorption spectrum was calculated from the reflectance spectrum using the Kubelka – Munk function [9]: $\alpha/S = (1 - R)^2/(2R)$ where α is the absorption coefficient, S is the scattering coefficient, which is practically wavelength-independent when the particle sizeis larger than 5 μm, and R is the reflectance. The NLO properties were tested on microcrystalline samples with particle size range 100–200 μm using an Nd:YAG laser (1064 nm) with an input pulse of 350 mV [26].

X-ray single-crystal diffraction data were collected on a Bruker P4 diffractometer with Mo Kα radiation (λ = 0.71073 Å) at 298 K using the θ–2θ scan technique and corrected for Lorentz – polarization and absorption corrections. The crystal structures were solved by direct method and refined by the full-matrix method based on F^2 by means of the SHELXLTL software package [27]. Non-H atoms were refined anisotropically using all reflections with $I > 2\sigma(I)$. All H atoms were generated geometrically and refined using a"riding" model with Uiso = 1.2 Ueq (C). The

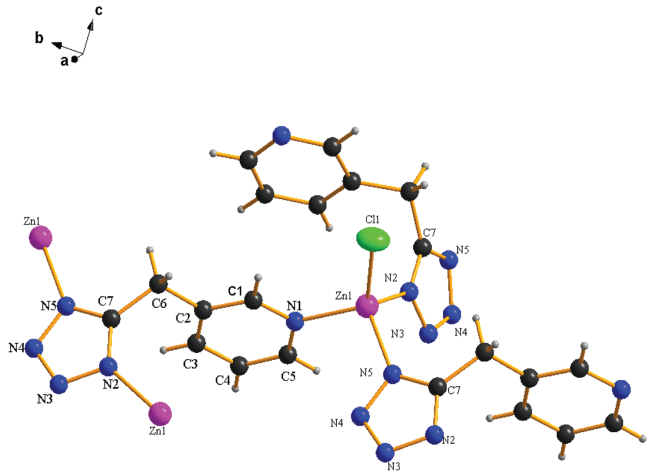

Fig. 1. Asymmetric unit view of **1** showing the Zn center located in highly distorted tetrahedral coordination geometry (30% thermal ellipsoids). Symmetry code: A: x-1/2, y-1/2, z; B: x, -y, z+1/2; C: -1/2+x, 1/2-y, -1/2+z.

asymmetric units and the packing views were drawn with DIAMOND (Brandenburg and Putz, 2005). Angles between some atoms were calculated using DIAMOND, and other calculations were performed using SHELXLTL. Crystal data and Structure refinements are listed in Table S1 (Supporting information). Their selected intra-atomic distances and bond angles are given in Table S2 (Supporting information). These data can be found on the Cambridge Crystallographic Data Centre at liberty *via* www.ccdc.cam.ac.uk/data_request/cif. CCDC No. 1048024 for **1**, No. 1048025 for **2**, No. 1048026 for **3**.

Single-crystal X-ray analyses reveal that complexes **1** and **2** are isomorphism and crystallizes in an acentric space group *Cc* (Table S1). Here we just described crystal structure of **1** at length. As shown in Fig. 1, each asymmetric unit in **1** contains one Zn ion, one chloride atom and one Tzmp- ligand. The coordination geometry around the central zinc can be best regarded as a distorted tetrahedron which was connected by one Cl atom, two α-N atoms from different tetrazole groups and one N atom from pyridyl group. The bond distance of Zn(1)-Cl(1) (2.1906(8) Å) is obviously longer than that of Zn(1)-N(5)#1 2.009(2), Zn(1)-N(1) 2.0117(18), Zn(1)-N(2)#2 2.0168(19) (Table S2), and all the bond angles (such as N(1)-Zn(1)-Cl(1) 115.36(7)) of the tetrahedron are deviated from 109.5°, suggesting that the central zinc metal in MOF **1** lies in a highly unsymmetrical fashion [8]. Each Tzmp- adopts a μ_3-η^1,η^1,η^1 tridentate coordination mode, bridging three Zn(II) atoms to form a co-edged double helical chain along the *a*-axis.

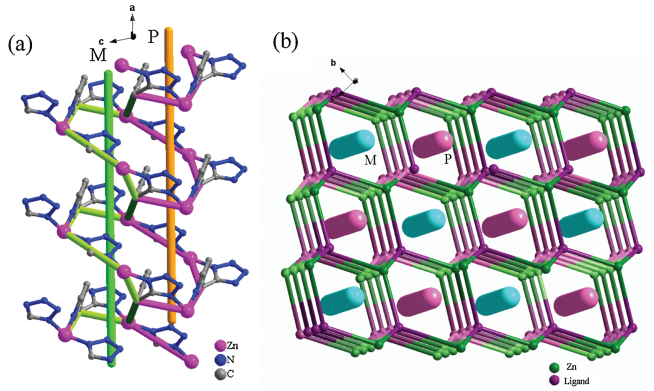

Fig. 2. (a) Co-edged double helical chain of **1** along the *a*-axis; (b) 3D topology network assembled from alternately arranged P and M co-edged double helical chains, the insert pillar indicate the helical axis.

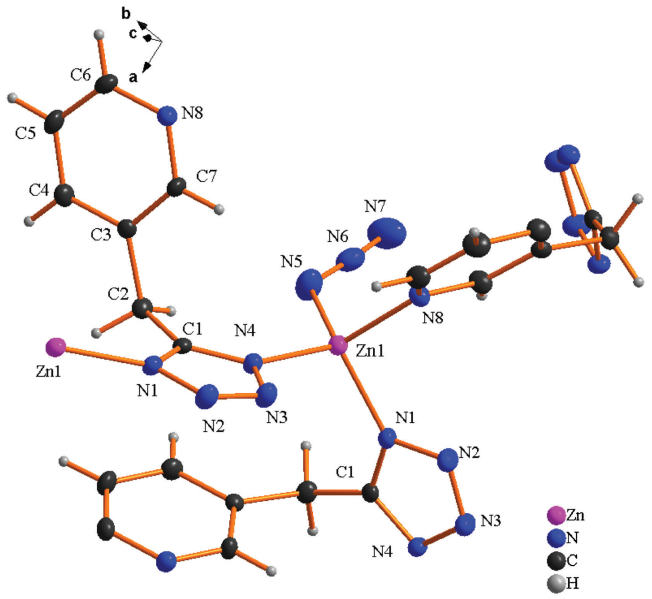

Fig. 3. Asymmetric unit view of **3** showing coordination geometry around Zn center (30% thermal ellipsoids). (Symmetrical code, A: 1.5-x, 0.5+y, z; B: 1-x, 0.5+y, 1.5-z; C: x, 1+y, z; D: 0.5+x, y, 1.5-z).

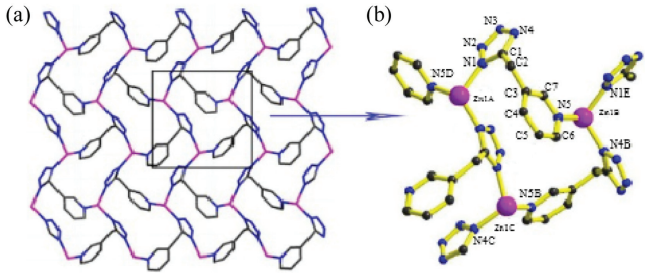

Fig. 4. (a) 2D framework structure of **3** viewed along the *c* axis, all the hydrogen atoms and N_3^- are deleted for clarity (the color for Zn: purple, N: blue and C: black); (b) the building block of **3** highlighted on Zn_3 $(Tzmp)_3$ unit (Symmetrical code, A:1.5-x, 0.5+y, z; B: 1-x, 0.5+y, 1.5-z; C: x, 1+y, z; D: 0.5+x, y, 1.5-z; E: -0.5+x, y, 1.5-z).

(Fig. 2a) The interweaved P and M double helical chains further parallel associated in the bc plane giving birth to the 3D acentric structure. (Fig. 2b) Simplifying the Zn(II) center and the averaged ligand as two three-connected topologically equivalent nodes affords an (3,3)-connected topology network which has an

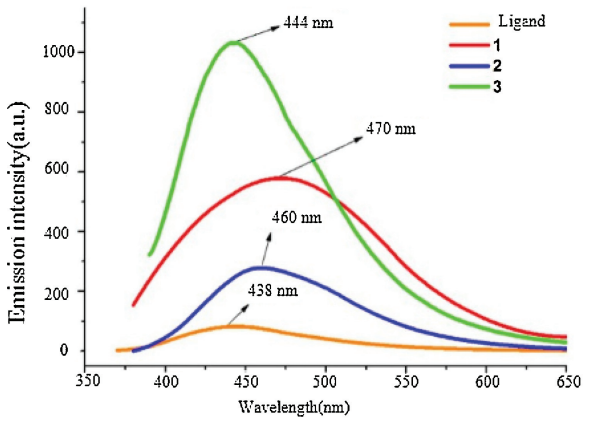

Fig. 6. Fluorescent emission spectra of **1**, **2**, **3** in solid state at room temperature.

extended Schäfli symbol of $10_2{\cdot}10_4{\cdot}10_4$ and a c10 number of 608 and is therefore a (10, 3)-b "ths" net [28,29]. (Fig. 2b)

The synthetic reaction conditions of **3** are very identical to that of **1** except $Zn(ClO_4)_2$ replace the $ZnCl_2$ while the structural difference comes that the N_3^- replace the position of Cl^- in **1**. As shown in Fig. 3, each asymmetric unit contains one Zn(II) ion, one N_3^- and one $Tzmp^-$ ligand. Similar to **1**, all the top net has two three-connected topologically equivalent nodes representing either the Zn(II) center (the auxiliary ligand N_3^- does not connect any other metals and can not be regarded as a bridging link too) or an averaged ligand position; however there are some great differences between them. On one hand, **1** and **3** crystallized in different space group, **3** belong to symmetric *Pbca* space group while **1** lies in an acentric space group *Cc*. What is more, the geometry of central Zn atoms in **1** are "seriously" distorted tetrahedron, while that in **3** are "slightly" distorted one, since all the Zn-N bonds distance are nearly equal from 1.921(3) Å to 2.034(2) Å in **3**. The building block of **3** can be regarded as $Zn_3(Tzmp)_3$ units (an 18-membered ring, Fig. 4b) which were connected with end to end fashion.The underlying topology is Shubnikov hexagonal plane net/(6, 3) (Fig. S3 in Supoprting information), and it can only extend along the *a* and *b* axes directions, therefore resulting in the formation of a sheet which paralleled to *ab* plane (Fig. 4a). To our knowledge, complexes with the same metal and ligand, even the same equivalent nodes but with dissimilar topologies are rarely reported before.

Why the similar subject, reaction conditions and coordination modes affords two structures with different space group, topologies and dimensionality? We suggest the following reason which can be

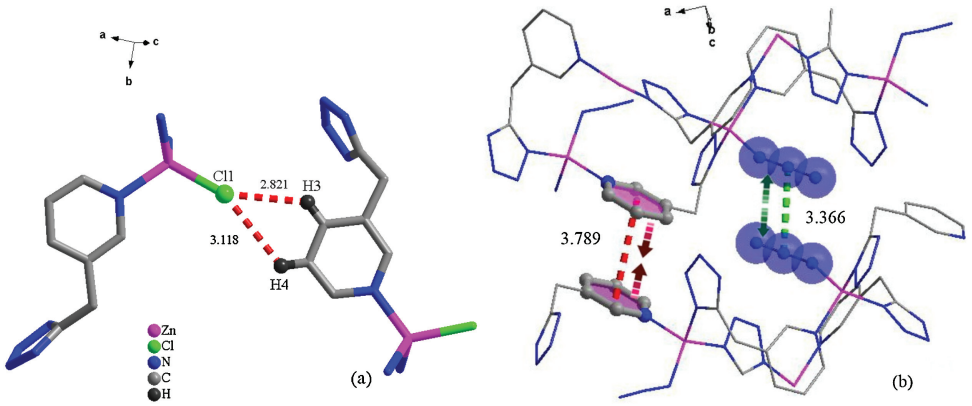

Fig. 5. (a) The weak hydrogen bonds attraction in **1** (or **2**). (b) The weak $\pi\cdots\pi$ interaction and repulsion force between the adjacent N_3^- group.

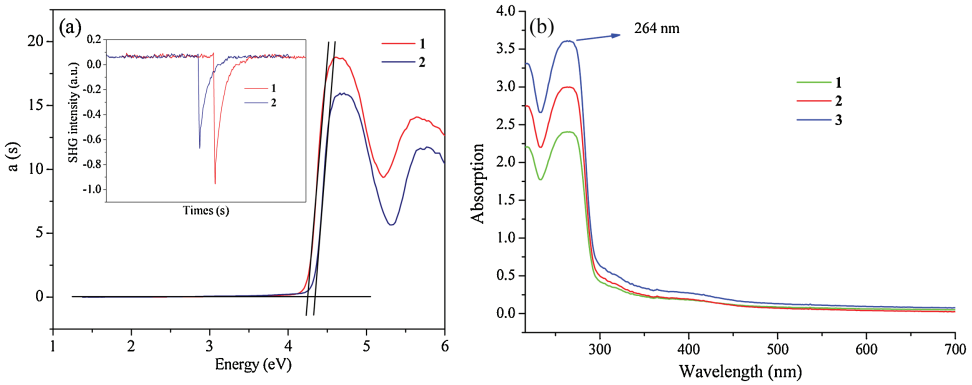

Fig. 7. (a) Optical diffusere flectance spectrums of **1** and **2**; Inset: the SHG signals of **1** and **2**; (b) Solid state UV absorption spectra of **1-3.**

explained for it: (i) The tetra- hedral intrinsically lacks a center of symmetry [16], further, the order parameter for the tetrahedral center of **1** (or **2**) is higher than **3**. That is one of the reasons for **1** (or **2**) crystallized in a lower symmetric noncentrosymmetric space group *Cc* while **3** in a higher symmetric centrosymmetric space group *Pbca*. (ii) The supermolecular interactions exist in **1** (or **2**) and **3** are different. There exist weak H-bonds attraction of C(3)-H(3)···Cl(1) (2.821 Å) and C(4)-H(4)···Cl(1) (3.118 Å) in **1** (Fig. 5a), although the hydrogen bond distance are obviously beyond a standard distance, electrostatic force majorly contributed the hydrogen bond effect [34–37]. In **3**, there posses both London attraction and Coulomb repulsion between the 2D sheet, the London attraction can be defined as the weak offset $\pi\cdots\pi$ interaction between adjacent pyridine groups with distance of 3.789 Å and dihedral angle of 0°. Another proof of $\pi\cdots\sigma$ attraction is the torsion angle between line of pyridine centres and the normal to the pyridine plane is 22.831°, a typic al offset $\pi\cdots\pi$ stocking [38]. Because of the high degree of overlap of electron cloud and a short distance (3.366 Å) of the adjacent N_3^- group, the interaction can be regarded as a repulsion (Fig. 5b) [32,38,39]. In another word, the bulky steric hindrance and electronegativity difference between N_3^- and halogen anion (Cl^-, Br^-) hindered the packing of **3** to form a compact structure compared to **1** (or **2**) [40,41].

As shown in Fig. 5, the room temperature solid-state fluorescence spectra of crystalline samples for **1**, **2**, **3** and HTzmp ligands were exhibited in Fig. 6. Title complexes **1**–**3** show an emission band centered at 470, 460 and 444 nm respectively, whereas the HTzmp ligand shows a maximal emission peaks around 438 nm, thus the photoluminescent mechanisms clearly attributed to ligand-to-1igand transitions (L→L) that are in reasonable agreement with the literature examples on this class of metal complex previously reported in our group and by others [5–9]. The emission maxima (λ_{max}) show the order of **1** < **2** < **3**, implying that the luminescence is influenced by the ligand-field strength of the negative ions ($N_3^- < Br^- < Cl^-$) [42–48]. It is thus believed that the electronic nature of the emissive excited states of **1**–**3** is affected to some degree by $X^-\rightarrow L$ (X^- = N_3^-, Br^- and Cl^-) charge transfer transitions.

The noncentrosymmetric crystal structure of **1** and **2** prompts us to examine their SHG responses. The results reveal that **1** and **2** display strong SHG efficiencies, approximately 2/3 and half of potassium respectively (Fig. 7a), indicating the obvious effects of push-pull effect (or one-center-A-D system) [5,49–51]. The coordination of the pyridyl and tetrazole rings to a metal center results in the donation of the lone pair of electrons on the N atoms to the metal center and the formation of an excellent donor acceptor (D-A) system. Furthermore the coordination of halogen atom (Cl, Br) to the metal center can effectively mediate the push-pull strength, presumably, the relatively higher electronegativity of Cl compared to Br leads to the stronger push-pull strength and more distinct SHG signal. The UV absorption spectrum of **1** and **2** indicates that they are transparent in the visible region with an absorption edge of 300 nm (Fig. 7b). The optical diffuse-reflectance study reveals an optical bandgap of 4.24 eV and 4.34 eV for **1** and **2**, making them a wide-band-gap semiconductor [16–19,52,53].

In summary, we have successfully trapped three novel Zn MOFs from flexible organic nitrile ligand by *in situ* [2 + 3] cycloaddition reactions and investigated the influence of the negative ions and underlying topologies on the crystal structure of metal-organic frameworks (MOFs). Their fluorescent properties are influenced by the ligand-field strength of the negative ions ($N_3^- < Br^- < Cl^-$). The strong SHG efficiencies and adjustable fluorescent emission properties indicate they may have potential applications in NLO and photoluminescent materials.

Acknowledgment

Prof. Tan is grateful for the support from the National Natural Science Foundation of China (Nos. 21761013, 21671086, 21766009).

Appendix A. Supplementary data

Supplementary material related to this article can be found, in the online version, at doi:https://doi.org/10.1016/j.cclet.2019.06.017.

References

[1] V.A. Blatov, L. Carlucci, G. Ciani, et al., CrystEngComm 6 (2004) 378–395.
[2] V.A. Blatov, M. O' Keeffe, D.M. Proserpio, CrystEngComm 12 (2010) 44–48.
[3] M. O' Keeffe, M.A. Peskov, S.J. Ramsden, et al., Acc. Chem. Res. 41 (2008) 1782–1789.
[4] A. Phan, C.J. Doonan, F.J. Uribe-Romo, et al., Acc. Chem. Res. 43 (2010) 58–67.
[5] H. Zhao, Z.R. Qu, H.Y. Ye, et al., Chem. Soc. R. 37 (2008) 84–100.
[6] Y.Z. Tang, M. Zhou, J. Huang, et al., Inorg. Chem. 52 (2013) 1679–1681.
[7] Y.Z. Tang, G.X. Wang, Q. Ye, et al., Cryst. Growth Des. 7 (2007) 2382–2386.
[8] Y.H. Tan, J.B. Xiong, J. Huang, et al., Chin. J. Inorg. Chem. 30 (2014) 1621–1628.
[9] X.M. Chen, M.L. Tong, Acc. Chem. Res. 40 (2007) 162–170.
[10] Y.W. Li, H. Ma, Y.Q. Chen, et al., Cryst. Growth Des. 12 (2012) 189–196.
[11] D. Tian, Q. Chen, Y. Li, et al., Angew. Chem. Int. Ed. 53 (2014) 837–841.
[12] K.H. He, W.C. Song, Y.W. Li, et al., Cryst. Growth Des. 12 (2012) 1064–1068.
[13] K.H. He, Y.W. Li, Y.Q. Chen, et al., Cryst. Growth Des. 12 (2012) 2730–2735.
[14] L. Li, S. Zhang, L. Han, et al., Cryst. Growth Des. 13 (2013) 106–110.
[15] H. Wang, W. Yang, Z.M. Sun, Chem. -Asian J. 8 (2013) 982–989.
[16] C. Wang, T. Zhang, W. Lin, Chem. Rev. 112 (2012) 1084–1104.
[17] S. Zhao, J. Zhang, S. Zhang, et al., Inorg. Chem. 53 (2014) 2521–2527.
[18] S. Zhao, P. Gong, S. Luo, et al., J. Am. Chem. Soc. 136 (2014) 8560–8563.
[19] L. Li, J. Ma, C. Song, M. Hong, et al., Inorg. Chem. 51 (2012) 2438–2442.
[20] H. Zhao, Z.R. Qu, H.Y. Ye, R.G. Xiong, Chem. Soc. Rev. 37 (2008) 84–100.
[21] Y.Z. Tang, J.B. Xiong, J.X. Gao, et al., Inorg. Chem. 54 (2015) 5462–5466.
[22] S.H. Wang, F.K. Zheng, M.J. Zhang, et al., Inorg. Chem. 52 (2013) 10096–10104.
[23] Y.Z. Tang, M. Zhou, H.R. Wen, et al., CrystEngComm 13 (2011) 3040–3045.
[24] J.X. Dong, H.L. Zhang, Chin. Chem. Lett. 27 (2016) 1097–1104.
[25] S.W. Kurtz, T.T. Perry, J. Appl. Phys. 39 (1968) 3798–3813.

[26] G.M. Sheldrick, SHELXS97, Program for Crystal Structure Solution, University of Gottingen, Gottingen, Germany, 1997.
[27] V. A. Blatov, D. M. Proserpio, A. R. Oganov, Modern Methods of Crystal Structure Prediction, Wiley-VCH, Berlin, 2011, pp. 1–28.
[28] A.B. Cory, R.H. Lyall, Cryst. Growth Des. 7 (2007) 1868–1871.
[29] A.F. Wells, Three-Dimensional Nets and Polyhedra, Wiley, New York, 1977.
[30] T. Hang, W. Zhang, H.Y. Ye, R.G. Xiong, Chem. Soc. Rev. 40 (2011) 3577–3598.
[31] W. Zhang, R.G. Xiong, Chem. Rev. 112 (2012) 1163–1195.
[32] S. Grimme, J.P. Djukic, Inorg. Chem. 50 (2011) 2619–2628.
[33] S. Kusaka, R. Sakamoto, Y. Kitagawa, M. Okumura, H. Nishihara, Chem. -Asian J. 7 (2012) 907–910.
[34] L. Adriaenssensa, P. Ballester, Chem. Soc. Rev. 42 (2013) 3261–3277.
[35] B. Schulze, U.S. Schubert, Chem. Soc. Rev. 43 (2014) 2522–2571.
[36] A.D. Bond, Cryst. Growth Des. 5 (2005) 755–771.
[37] F. Wang, H. Du, H. Liu, X. Gong, Chem. -Asian J. 7 (2012) 2577–2591.
[38] Y.H. Tan, J.B. Xiong, J.X. Gao, et al., RSC Adv. 5 (2015) 30216–30221.
[39] Z. Chen, A. Lohr, C.R. Saha-Möller, F. Würthner, Chem. Soc. Rev. 38 (2009) 564–584.
[40] P. Liu, L. Xiang, Q. Tan, H. Tang, H. Zhang, Polym. Chem. 4 (2013) 1068–1076.
[41] Y.L. Wang, N. Zhou, Y. Ma, et al., CrystEngComm 14 (2012) 235–239.
[42] M. Hashimoto, S. Igawa, M. Yashima, et al., J. Am. Chem. Soc. 133 (2011) 10348–10351.
[43] J.L. Chen, X.F. Cao, J.Y. Wang, et al., Inorg. Chem. 52 (2013) 9727–9740.
[44] M.T. Buckner, T.G. Matthews, F.E. Lytle, D.R. McMillin, J. Am. Chem. Soc. 101 (1979) 5846–5848.
[45] M.W. Blaskie, D.R. McMillin, Inorg. Chem. 19 (1980) 3519–3522.
[46] D. Song, W.L. Jia, G. Wu, S. Wang, Dalton Trans. 6 (2005) 433–438.
[47] E. Wong, J. Li, C. Seward, S. Wang, Dalton Trans. 7 (2009) 1776–1785.
[48] M.G. Crestani, G.F. Manbeck, W.W. Brennessel, T.M. McCormick, R. Eidenberg, Inorg. Chem. 50 (2011) 7172–7188.
[49] Q. Ye, Y.H. Li, Y.M. Song, et al., Inorg. Chem. 44 (2005) 3618–3625.
[50] D.W. Fu, W. Zhang, R.G. Xiong, Cryst. Growth Des. 8 (2008) 3461–3464.
[51] Y. Li, G. Xu, W.Q. Zou, et al., Inorg. Chem. 47 (2008) 7945–7947.
[52] Q. Wei, J.W. Cheng, C. He, G.Y. Yang, Inorg. Chem. 53 (2014) 11757–11763.
[53] P. Kubelka, F.Z. Munk, Tech. Phys. 12 (1931) 593–601.